ROYAL SOCIETY OF CHEMISTRY

PAPER

Check for updates

Supercritical CO$_2$-foamed polystyrene composites containing wood-derived biochar for sustainable thermal insulation

Apurv Gaidhani, Guoshan Min, Lauren Tribe and Paul Charpentier*

Building insulation materials with low environmental impact are critical for reducing energy use and greenhouse gas emissions. In this study, sustainable polystyrene (PS) composite foams were developed by incorporating wood-derived biochar (0–7.5 wt%) using supercritical CO$_2$ (sc-CO$_2$) extrusion. The foam containing 2.5 wt% biochar (BC) exhibited the smallest average cell size ($\sim$86 μm), highest cell density ($\sim$3.3 × 10^8 cells per cm^3), and narrowest cell size distribution. Correspondingly, its thermal conductivity decreased from 36 to 32 mW m^{-1} K^{-1} ($\approx$11% reduction), while the specific compressive strength reached 3.9 MPa g^{-1} cm^3, approximately 100% higher than pristine PS foam. Transmission electron microscopy confirmed uniform BC dispersion and localization along cell walls, indicating its role as an effective nucleating agent. Micro-computed tomography (micro-CT) further verified increased BC content and distribution in the 2.5 wt% foam, supporting the observed improvements in cellular structure and performance. These results demonstrate that BC effectively enhances the foaming behavior, thermal insulation and mechanical performance of the composite. Furthermore, comparative embodied carbon and thermal resistance analyses indicate that BC addition improves the overall environmental sustainability and promotes circular material use in PS−BC composite foams, offering a scalable pathway for developing next-generation sustainable insulation materials.

Sustainability spotlight

This research advances sustainable materials design by developing PS composite foams using BC derived from wood waste and sc-CO$_2$ as a green, non-toxic foaming agent. Upcycling BC not only diverts wood waste biomass from landfills but also sequesters carbon in durable foams, offering significant environmental benefits. The resulting lightweight, load-bearing insulation materials improve building energy efficiency, reducing greenhouse gas (GHG) emissions and supporting the transition to low-carbon, green buildings. This work aligns directly with UN SDG 11 (Sustainable Cities and Communities) and SDG 13 (Climate Action) by lowering urban energy demands and mitigating climate impacts. Furthermore, by valorizing renewable biomass and employing clean processing with sc-CO$_2$, this approach also supports SDG 12 (Responsible Consumption and Production). Together, these innovations present a scalable pathway toward climate-resilient, resource-efficient construction materials.

1 Introduction

Polystyrene (PS) foams remain indispensable in insulation, packaging, and lightweight structural applications due to their unique combination of low density, good thermal resistance, and cost-effectiveness.[1–5] These cellular materials effectively minimize conductive and convective heat transfer, offering high energy-saving potential in both residential and industrial buildings.[6,7] In cold or temperate regions, where space heating constitutes a significant portion of total energy demand, the role of insulation materials becomes particularly critical.[8–10] Recent analyses by the International Energy Agency report that buildings account for nearly 35% of total final energy consumption and approximately 38% of energy-related greenhouse gas (GHG) emissions, much of which arises from heating and cooling requirements.[11,12] Enhancing insulation performance can reduce energy consumption in buildings by 30–50%, depending on climatic conditions and building envelope quality.[13,14] Consequently, developing sustainable, high-efficiency insulation materials is essential to achieving the United Nations Sustainable Development Goals (SDGs), notably SDG 11 (Sustainable Cities and Communities) and SDG 13 (Climate Action), both of which emphasize the importance of energy efficiency, climate resilience, and the transition to circular materials.

Despite their widespread use, conventional PS foams are petroleum-derived and contribute significantly to the embodied carbon footprint of the built environment.[15] Their production involves fossil-based monomers and energy-intensive processes, while their end-of-life disposal poses environmental challenges

Department of Chemical and Biochemical Engineering, University of Western Ontario, London, Ontario, N6A 5B9, Canada. E-mail: pcharpen@uwo.ca

due to poor recyclability and persistence in landfills.[16] This has driven growing interest in integrating bio-based fillers and additives that can partially displace fossil carbon while maintaining desirable physical and mechanical performance. In particular, carbonaceous fillers derived from renewable sources offer a promising route to enhance the sustainability of polymer foams. Biochar (BC), a porous, carbon-rich residue generated *via* pyrolysis of biomass under oxygen-limited conditions, has emerged as one of the most promising materials for this purpose.[17–20] Its inherent characteristics including low thermal conductivity, high surface area, tunable pore structure, and high carbon stability, make it an attractive candidate for use in polymer composites and foam systems.[21,22] Moreover, BC can be produced from low-value forestry residues and agricultural wastes, contributing to waste valorization and carbon sequestration while aligning with circular-economy principles.[23]

The integration of BC into polymeric matrices has been shown to improve thermal, mechanical, and morphological properties in a variety of systems. Studies have demonstrated that BC particles can act as nucleating sites during foaming, leading to finer and more uniform cell structures.[24,25] Their low intrinsic thermal conductivity can enhance insulation performance by disrupting heat flow pathways.[26] For instance, BC derived from rice husks, coconut shells, and pine sawdust has been reported to reduce the thermal conductivity of polymer composites while increasing stiffness and thermal stability.[27–29] These effects make BC a sustainable alternative to conventional carbon fillers such as graphite, carbon black, or carbon nanotubes, which are costly and energy-intensive to produce. Additionally, life-cycle assessment (LCA) studies indicate that BC use in composites can result in a net reduction of cradle-to-gate global warming potential (GWP), as it locks biogenic carbon within durable materials and offsets emissions associated with fossil-based fillers.[30,31]

Despite the growing interest in sustainable polymer foams, most reported studies on BC–polymer systems have focused on biodegradable matrices such as polylactic acid (PLA) or polyurethane, typically using batch foaming methods under supercritical CO_2 or chemical blowing agents.[32–34] While convenient for laboratory-scale investigations, batch foaming inherently suffers from small sample volumes and often produces poorly interconnected cell structures.[35,36] Consequently, such studies do not capture the processing dynamics relevant to industrial foam production and thus limit scalability.[37] Moreover, limited research has examined PS reinforced with BC, despite PS's dominance in insulation applications, leaving the dual role of BC as both a nucleating agent influencing cellular structure and a carbonaceous filler contributing to environmental benefits underexplored. To address these gaps, the present study employs a pilot-scale continuous supercritical CO_2 (sc-CO_2) extrusion foaming line, a safe, solvent-free, and industrially relevant process that closely replicates real manufacturing conditions. This continuous system enables steady-state operation, controlled gas diffusion, and reproducible processing parameters, leading to more uniform cell structures and data directly translating to large-scale production. By coupling this advanced foaming approach with detailed microstructural and environmental (cradle-to-gate GWP) evaluations, this work

provides new insights into the structure–property relationships and sustainability potential of PS–BC composite foams, advancing their transition from laboratory research to viable, low-carbon insulation materials.

In this study, we introduce wood-derived BC from oak and maple sawdust into PS foams at loadings ranging from 0 to 7.5 wt%, produced using sc-CO_2 in a pilot-scale continuous extrusion process. The morphology of the resulting foams was characterized using scanning electron microscopy (SEM) to investigate cell morphology. Structural parameters such as average cell size, and cell density were quantified, and cell size distribution was evaluated qualitatively to build structure–property correlations with measured thermal conductivity and compressive mechanical properties. BC dispersion and presence in the polymer matrix was assessed with the help of advanced characterization techniques such as transmission electron microscopy (TEM) and micro computed tomography (micro-CT). Beyond performance characterization, a comprehensive environmental comparison was conducted using cradle-to-gate GWP data for all major material components. The environmental and performance outcomes were benchmarked side-by-side with conventional foams to evaluate trade-offs between functionality and sustainability. This integrated approach, combining pilot-scale processing, morphological analysis, and environmental assessment, reveals how BC enhances structural performance and sustainability in low-carbon PS insulation foams, supporting materials aligned with the circular economy and the UN SDG.

2 Experimentation

2.1 Materials

Biochar (BC), produced *via* pyrolysis of maple and oak sawdust, was kindly provided by Airex Energy (Quebec, Canada). Polystyrene (PS 595 T) with a melt flow index (MFI) of 1.6 g 10 min^{-1} (200 °C, 5 kg) and a density of 1.04 g cm^{-3} was purchased from Total Energies Petrochemicals & Refining (USA). The blowing agent, carbon dioxide (CO_2, 99.9% purity), was supplied by Linde Canada. Talc powder (JetWhite 1HC, median particle size 1.1 μm) was kindly donated by Magris Talc (USA).

2.2 Extrusion foaming of PS and PS–BC composites

Extrusion foaming of pristine PS and PS–BC composites was carried out on a pilot-scale twin-screw extruder (Feininger SHJ-Z36 × 25, D = 36 mm, L/D = 25, throughput = 3 kg h^{-1}) using sc-CO_2 as the physical blowing agent. The PS–BC composite foams were prepared using a two-stage supercritical CO_2 (sc-CO_2) extrusion process. The primary extrusion stage involved melt compounding and initial mixing of PS and BC, conducted at temperatures of 190 °C (feed zone), 195 °C (compression zone), and 190 °C (metering zone). In the secondary extrusion stage, where CO_2 was injected and foaming occurred, the temperature profile was reduced to 130 °C, 195 °C, and 165 °C, respectively, while the die zone temperature was maintained at 140 °C. The process operated at a screw speed of 50 rpm, with ambient cooling and an sc-CO_2 pressure of 17.3 MPa. All

formulations contained 1 wt% talc as a nucleating agent. Pristine PS was dry-blended with oak and maple wood-derived BC at four concentrations (1, 2.5, 5, and 7.5 wt%) prior to extrusion, and the resulting mixtures were melt-processed in the extruder at a sc-CO_2 pressure of 17.3 MPa to produce foams. The processing and foaming procedure for PS composite foams is described in detail in our previous work.[38] A schematic overview of the extrusion foaming process is presented in Fig. 1.

2.3 Characterization

2.3.1 Density and morphological analysis. Foam density was calculated using ASTM D1622. Three specimens were tested for each composite foam sample and the average value is reported. The test specimens were rectangular in shape ($23 \times 8 \times 7$ mm). The foam skin was removed prior to the measurements, and an average of three readings was considered for the final reported value. Expansion ratio of foam (ϕ) was calculated as

$$\phi = \frac{\rho_{\text{solid}}}{\rho_{\text{foam}}} \quad (1)$$

where ρ_{solid} is the bulk density of the solid polymer composite and ρ_{foam} is the density of the foam. The porosity of the foam samples was calculated by using the following equation:

$$\text{Porosity}(\%) = \left(1 - \left(\frac{\rho_{\text{foam}}}{\rho_{\text{solid}}}\right)\right) \times 100$$
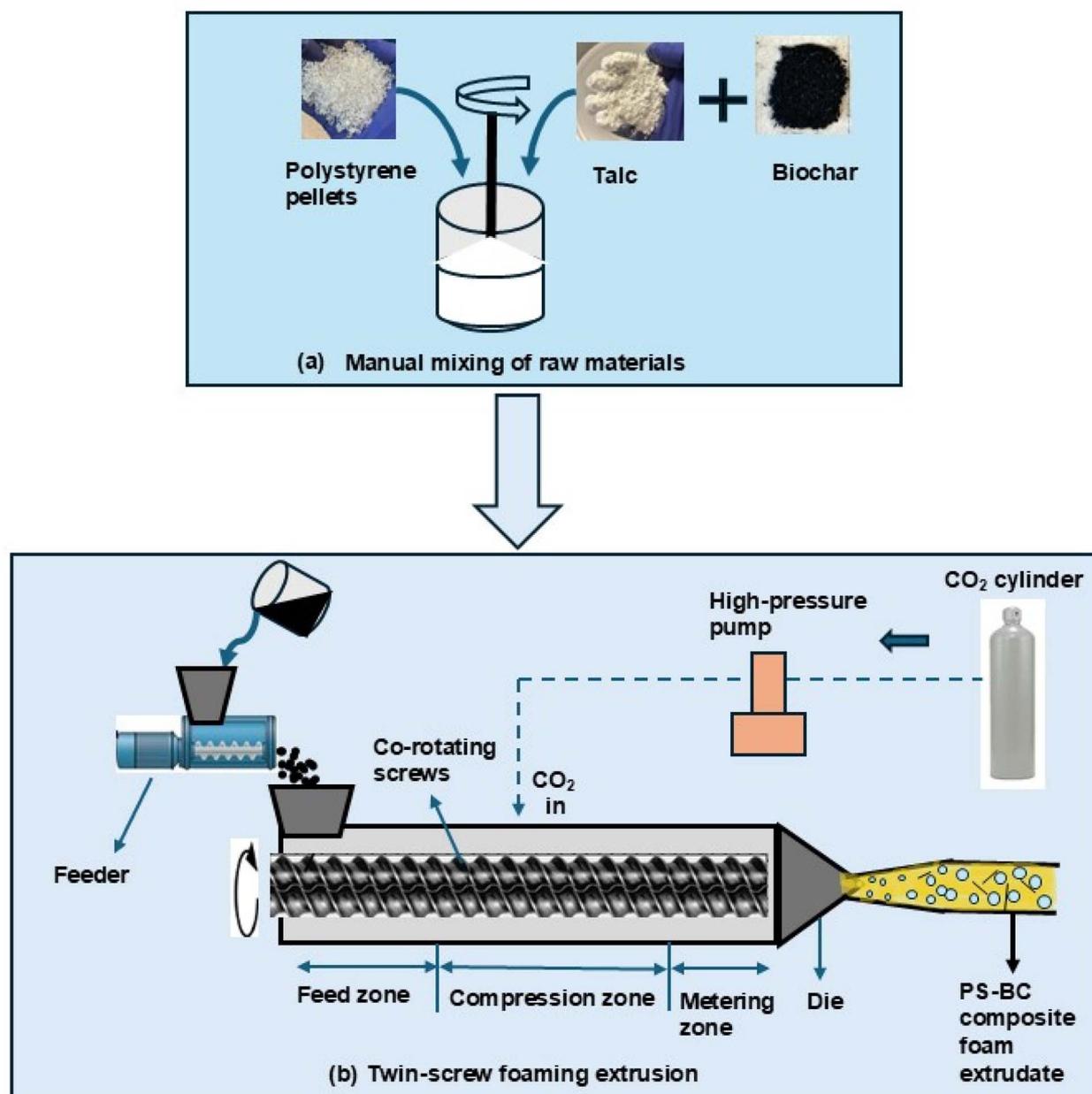

Fig. 1 Two step preparation process of PS–BC composite foam (a) manual mixing followed by (b) twin-screw foaming extrusion.

Morphological analysis of the PS–BC composite foams was performed using a Scanning Electron Microscope (SEM, Hitachi Flex SEM 1000 II) operating at a voltage of 5 kV was used to examine the foam morphologies. The foam samples were freeze-fractured in liquid nitrogen, and observations were carried out along the direction perpendicular to the extrusion at the center of the foam width after removal of the skin. Fiji (ImageJ) software was used for cell size and particle size analysis, utilizing SEM pictures with a magnification ratio of 50. Cell size was calculated as the average diameter of all cells in a SEM picture. Subsequently, the cell density (N_0) was calculated:

$$N_0 = \left(\frac{n}{A}\right)^{\frac{3}{2}}\phi \qquad (2)$$

where n is the number of cells in a SEM picture, A is the area of the SEM picture and N_0 is the number of cells per unit volume. Cell and particle size distribution were plotted using histograms and Gaussian fitting. Cells per unit volume. Cell size distribution was plotted using a histogram and Gaussian fitting.

The open cell content of the foam samples was determined using a micrometrics Accupyc II 1340 (Foampyc) gas pycnometer with nitrogen as a penetrating fluid. The volume of displaced N_2 gas estimates the volume of open cells. The test was conducted on a rectangular solid of dimensions 2.1 × 0.7 × 0.5 cm, and an average of three readings was reported. The open cell content (%) was calculated:

$$\text{Open cell content (\%)} = (V_{\text{open cell}}/V_{\text{geo}}) \times 100$$

where $V_{\text{open cell}}$ is the volume of open cells and V_{geo} is the geometric volume of the foam sample tested.

2.3.2 Thermal and mechanical properties. Thermal conductivity of the foams was evaluated under steady-state conditions using a Heat Flow Meter (HFM) apparatus (Fox 200, TA Instruments, LaserComp). Compressive behavior was examined under strain-controlled loading with a vertical compression setup (Instron Model 5943) equipped with a 1 kN load cell, controller panel, and parallel upper and lower platens. The compressive modulus was calculated from the initial linear portion of the stress–strain curve, while the compressive strength corresponded to the stress at 10% strain. Each composite foam was tested using seven rectangular samples (16 × 16 × 7 mm), and the reported results represent the average values. Prior to loading, a 2 N axial pre-load was applied to ensure uniform contact. Compression was performed at a constant crosshead speed of 0.7 mm min^{-1} until 50% strain. All tests followed the ASTM D1621 procedure, except for the reduced specimen thickness necessitated by the limited dimensions of the extruded foams. The specific compressive modulus and strength were obtained by normalizing the measured values by the corresponding foam densities.

2.3.3 Dispersion studies. Transmission electron microscopy (TEM) images were acquired on a JEM 1200 EX microscope (JEOL, USA) operating at a voltage of 80 kV. Prior to acquiring images, pieces of the foam samples were embedded in Spurr's epoxy resin and polymerized overnight at 60 °C. Thin sections

were sliced on an ultramicrotome (Leica UCT) and picked up onto copper grids for viewing under the microscope. The samples were trimmed into rectangular pieces that were suitable for micro-CT analyses. The micro-CT was a Zeiss Xradia 410 Versa. Micro-CT involves passing X-rays through a sample volume and detecting the intensities of the transmitted X-rays. Variations in the sample volume density, such as voids or cracks, cause variations in the X-ray absorption that are expressed as differing greyscale values in the projected image (X-ray radiometric projection image). Multiple projection images are captured at different angles and were subsequently reconstructed into a 3D dataset. Following the acquisition of the datasets, each was processed in Object research system's dragonfly pro software and presented as 2D cross-sections and 3D cubes.

2.3.4 Biochar characterization. For optical microscopy, a small amount of BC was dispersed in ethanol, and a drop of the resulting suspension was placed on a glass slide for imaging. For SEM analysis, the particles were uniformly mounted on conductive carbon tape, and excess loosely attached powder was removed by gentle air blowing. Optical micrographs (4×) and SEM images (50×), each containing scale bars, were captured and processed using Fiji (ImageJ) software to evaluate the particle size distribution.[36] FTIR analysis was conducted using a Nicolet 6700 spectrometer (Thermo Scientific) across a wavenumber range of 600–4000 cm^{-1}. Nitrogen adsorption–desorption measurements were performed at −196 °C using a constant-volume adsorption analyzer (Tristar ASAP 2020, Micromeritics Instrument Corp., Norcross, GA, USA) with 99.995% pure N_2 and He (Praxair, Oakville, ON, Canada) to determine the Brunauer–Emmett–Teller (BET) surface area, pore volume, and pore diameter. Samples were degassed at 105 °C for 12 h prior to testing, and the pore size distribution was obtained from the desorption branch using the Barrett–Joyner–Halenda (BJH) method. Elemental composition was analyzed *via* energy-dispersive X-ray spectroscopy (EDX) coupled to an SEM (Hitachi SU3500) operating at 20 kV. BC powders were mounted uniformly on carbon tape to ensure complete surface coverage before analysis. EDX spectra were collected from six randomly selected regions, and the averaged values are reported.

3 Results and discussion

3.1 Characterization of biochar

The surface properties and elemental composition of BC influence its performance as a reinforcing filler and nucleating agent in polymer composites.[39] As shown in Table S1, the wood-derived BC exhibits a specific surface area (SSA) of 33 m^2 g^{-1}, a mean pore size (PS) of 3.7 nm, and a pore volume (PV) of 0.031 cm^3 g^{-1}, while elemental-EDX analysis reveals approximately 84.6% C, 10.9% O, 0.1% Mg, 1.5% K and 2.7% Ca. This composition is consistent with existing reports for woody feedstock BC, where high carbon content and modest oxygen content reflect the condensed aromatic framework typical of wood-derived chars. For example, Domingues et al.[40] noted that wood and sugar-cane derived BC had higher C concentrations

RSC Sustainability

Paper

and lower ash-related inorganic elements than nutrient-rich feedstocks. Additionally, Gezahegn et al.[41] observed that alkaline elements such as Mg, Ca and K are present in wood-biomass derived chars, and these elements contribute to the pH and ash signature of the final BC. The relatively small pore size and low pore volume reflect limited activation or moderate pyrolysis condition,[42] but still afford a significant surface area which supports adsorption or nucleation functions in composite applications. Combined, the chemical and textural attributes of this BC make it a suitable platform for heterogeneous nucleation, gas adsorption (such as CO_2), and interface interactions in polymer composite foaming systems.

FTIR spectra of oak- and maple-derived BC (Fig. S1) display peaks at 1770, 1480, and 905 cm^{-1}, corresponding to C=O stretching, aromatic C=C stretching, and out-of-plane C–H bending, respectively. A weak band near 3700 cm^{-1} indicates free O–H groups or adsorbed moisture, potentially reflecting a higher pyrolysis temperature. The peak at 1321 cm^{-1} is assigned to phenolic O–H vibrations, while the band around 660 cm^{-1} corresponds to out-of-plane C–OH or aromatic C–H deformations.[43,44] BC particle size was characterized using both scanning electron microscopy (SEM) and optical microscopy. SEM images of dry, well-separated BC particles (Fig. S2(a)) provided a mean particle size of 112 μm, reflecting individual particle dimensions with minimal agglomeration. In contrast, optical microscopy of ethanol-dispersed samples (Fig. S2(b)) showed larger mean particle sizes of 212 μm due to the presence of visible agglomerates, which were measured as single, larger particles. The difference in measured sizes highlights the influence of sample preparation and dispersion state on particle size analysis, with SEM offering a more accurate assessment of individual particle dimensions.

3.2 Cellular morphology of PS–BC composite foams

3.2.1 Foaming expansion behavior. The influence of BC loading on the foaming expansion behaviour and open-cell structure of PS foams produced via sc-CO_2 extrusion is summarised in Fig. 2 and Table 1. The pristine PS foam exhibited a density of 101 kg m^{-3} and porosity of 90.3%, corresponding to an expansion ratio of approximately 10. Incorporation of 1 wt% BC decreased the foam density to 85 kg m^{-3} and increased porosity to 91.8, indicating that BC particles acted as efficient heterogeneous nucleation sites, promoting uniform bubble formation and gas expansion. At 2.5 wt% BC, the density increased to 108 kg m^{-3} while porosity slightly decreased to 89.7%, accompanied by a sharp reduction in open-cell content (18.8%). This suggests that increased filler content elevated melt viscosity,[45] restricted gas diffusion, and hindered bubble coalescence, leading to a predominantly closed-cell morphology. The optimum expansion was achieved at 5 wt% BC, where the foam exhibited the lowest density (83 kg m^{-3}) and highest porosity (92.1%). This composition also showed the lowest open-cell fraction (13.5%), suggesting that stabilised cell walls suppressed rupture, resulting in maximised cell growth without significant interconnection.[46] Further addition of 7.5 wt% BC again raised the density (108 kg m^{-3}) and reduced porosity
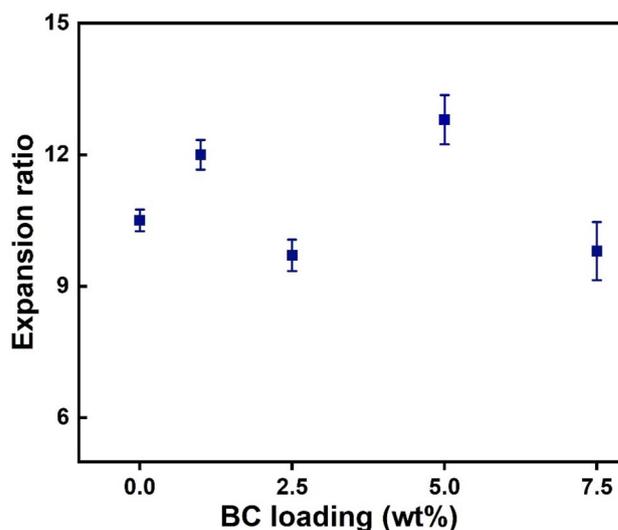

Fig. 2 Variation in expansion ratio of PS–BC composite foams.

(89.9%), while slightly increasing open-cell content (17.6%) possibly due to agglomeration-induced nonuniform nucleation.

Collectively, these findings reveal a non-monotonic trend in foam density and open-cell content with BC loading. Low-to-moderate filler levels (1–5 wt%) enhance nucleation and CO_2 expansion, whereas higher loadings hinder bubble growth due to rheological constraints. Overall, the foams are highly porous, with porosity values ranging from approximately 89 to 92%, confirming that the materials maintain a lightweight structure suitable for thermal insulation applications.[47] Moreover, the presence of BC decreased the open-cell content overall, particularly at ≥2.5 wt%, reflecting improved cell-wall integrity and increased closed-cell character. As the open-cell fraction directly influences the thermal conductivity of foams, by altering the pathways for gaseous and radiative heat transfer,[48] further discussion on its impact is provided in Section 3.4. These results align with prior studies on BC-filled polymer foams, where density and expansion exhibit similar non-linear behavior. For instance, Haham et al.[32] observed reduced foam density and increased expansion in PLA foams at 1 wt% BC loadings, followed by densification at higher concentrations. Likewise, Uram et al.[34] reported up to a 20% decrease in apparent density and enhanced closed-cell morphology in BC-modified polyurethane foams. Representative images of the PS–BC composite foams are presented in Fig. 3.

Table 1 Cellular structure parameters of PS–BC composite foam, showing measured apparent density, open-cell content, and calculated porosity at different BC loadings

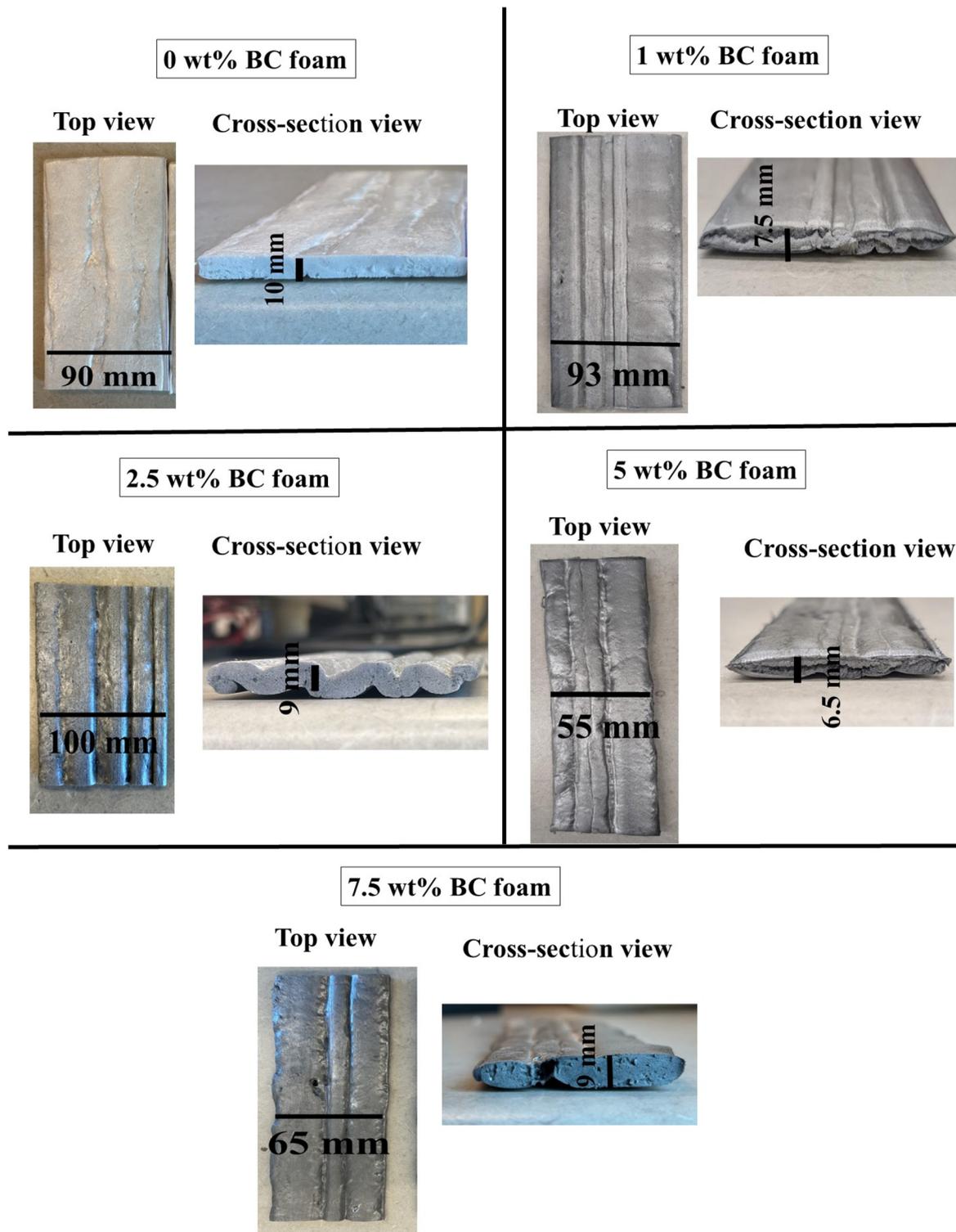| BC (wt%)	Apparent density (kg m^{-3})	Open cell content (%)	Porosity (%)
0 (pristine PS)	101 ± 10	40.4 ± 2.1	90.3 ± 0.9
1.0	85 ± 4	45.8 ± 2.3	91.8 ± 1.7
2.5	108 ± 6	18.8 ± 1.4	89.7 ± 0.6
5.0	83 ± 5	13.5 ± 1.7	92.1 ± 1.0
7.5	108 ± 7	17.6 ± 1.2	89.9 ± 1.1

Fig. 3 Representative images of PS–BC composite foams.

3.2.2 Effect of BC loading on the nucleation in PS composite foam. According to the classical nucleation theory, the introduction of solid particles into a polymer matrix can significantly reduce the free energy barrier required for bubble formation during foaming, thus leading to heterogeneous nucleation.[49,50] The nucleating particles act as energetically favorable sites that facilitate gas molecule accumulation and subsequent cell nucleation. This reduces the critical radius for stable bubble formation, thereby promoting the generation of a larger number of smaller bubbles. Consequently, the foam exhibits a higher cell density and a narrower cell size distribution. The role of carbon additives in lowering the free energy

barrier was explained in detail with the help of equations in our previous work.[38]

The cellular morphology of PS–BC composite foams produced *via* sc-CO_2 extrusion is shown in Fig. 4, where representative SEM micrographs (Fig. 4a) and corresponding cell size distributions (Fig. 4b) highlight the evolution of cell structure with increasing BC loading. The pristine PS foam exhibited large, irregular cells with an average size of approximately 220 μm and a broad distribution, characteristic of limited nucleation and uncontrolled bubble growth, resulting in a cell density of about 1.4×10^8 cells per cm^3. Upon the addition of 1 wt% BC, the average cell size decreased significantly (∼95 μm), and the cell density increased to ∼2.6×10^8 cells per cm^3,

indicating that BC particles acted as efficient heterogeneous nucleating agents during CO_2 foaming. The presence of finely dispersed nucleation sites at this loading facilitated uniform gas bubble initiation and a more refined, well-defined cellular structure. With 2.5 wt% BC, the foam displayed the smallest average cell size (∼86 μm) and the highest cell density (∼3.3×10^8 cells per cm^3), along with the narrowest cell size distribution, confirming the strongest nucleation effect and the formation of a highly uniform and stable cellular network. This trend suggested that BC at moderate loading levels may have effectively lowered the free energy barrier for bubble formation, thereby possibly enhancing CO_2 nucleation and cell uniformity. However, at higher BC contents (5 and 7.5 wt%), a slight
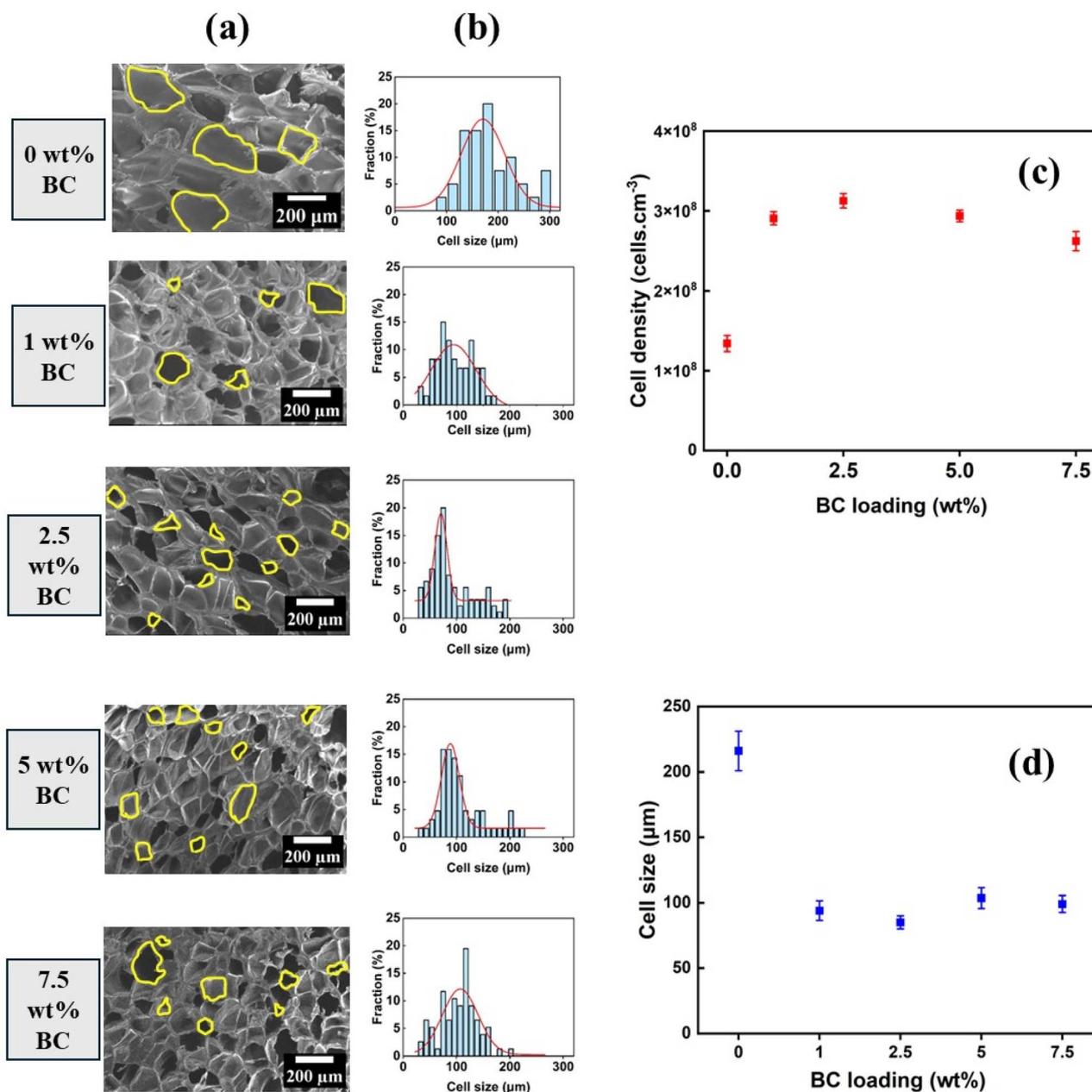

Fig. 4 (a) SEM micrographs. (b) Corresponding cell size distributions, (c) average cell sizes, (d) cell densities of PS−BC composite foams extruded using sc-CO_2 (note: yellow outlines indicate selected bubble cells).
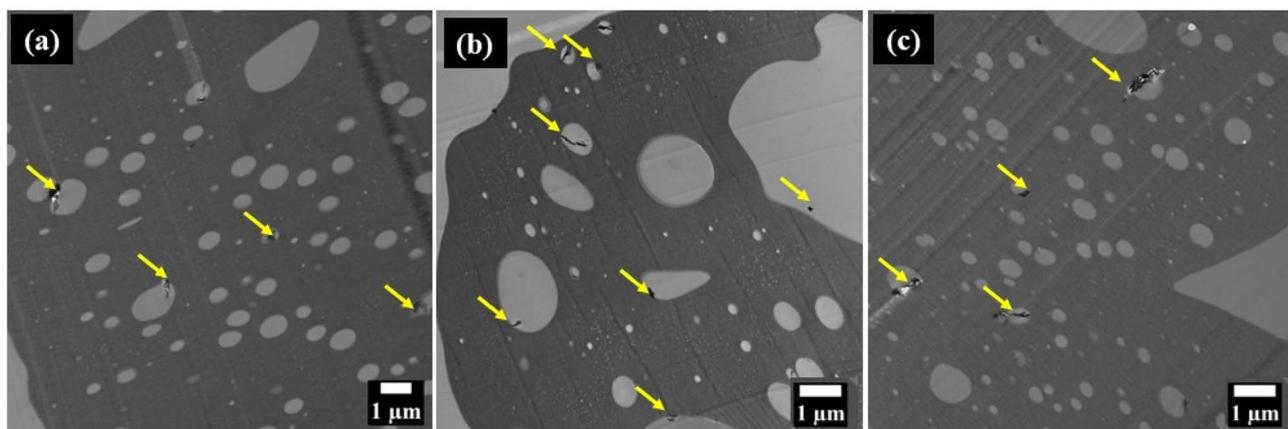
Fig. 5   TEM images of PS composite foam (a) 1 wt% BC, (b) 2.5 wt% BC and (c) 5 wt% BC (note: yellow arrows represent BC particles).

enlargement of the cells and a marginal decrease in cell density were observed, which may be attributed to increased melt viscosity and possible filler agglomeration that limit gas diffusion and uniform nucleation. Overall, these results confirm that BC serves as an efficient nucleating agent at low to moderate concentrations (1–2.5 wt%), promoting the development of small, uniform cells and high cell density, while excessive loading tends to disrupt the delicate balance between nucleation and cell growth, leading to partial loss of cellular uniformity. Previous studies have similarly demonstrated the effective role of BC as a heterogeneous nucleating agent in polymer foams and composites.[32,51]

3.3   Transmission electron microscopy (TEM) and micro-CT studies

TEM images of the foamed PS composites containing different loadings of BC are presented in Fig. 5. The presence of carbon-rich regions, indicated by yellow arrows, confirmed the successful incorporation of BC particles within the polymer matrix for all formulations. The particles appear well-dispersed, with no significant agglomeration observed even at the highest loading of 5 wt% BC. Notably, many BC particles were located at or near the edges of the polymer cells, consistent with their potential role as nucleation sites during foaming. Overall, these TEM observations demonstrate both the effective incorporation and uniform distribution of BC within the PS matrix, supporting its function in influencing cell formation and morphology.

The 2D reconstructed micro-CT cross-sections and corresponding 3D volume renderings of the PS–BC composite foams are presented in Fig. 6. Micro-CT analysis was performed specifically on the 1 wt% and 2.5 wt% BC foams because these two formulations exhibited the lowest thermal conductivity and highest specific compressive strength values among the tested samples (as discussed in Section 3.4). These images provide clear visual and quantitative evidence of BC distribution within the cell walls. In the 1 wt% BC foam (Fig. 6a and c), only a limited number of high-density regions appear (highlighted by yellow arrows), indicating sparse BC clusters embedded within the polymer matrix. In contrast, the 2.5 wt% BC foam

(Fig. 6b and d) exhibits a noticeably larger number of high-attenuation red regions, confirming a higher concentration of carbon-rich BC particles dispersed along the cell walls and struts. This trend is consistent with the micro-CT-derived volume fractions, where the BC content increased from 0.2% in the 1 wt% BC foam to 0.8% in the 2.5 wt% BC foam, while the PS matrix fraction increased from 3.0% to 3.9% (Table 2). The quantitative volume-fraction results corroborate the visual observations, validating that the 2.5 wt% BC foam contains a greater amount of BC and a more continuous distribution within the foam microstructure.

This enhanced presence of BC at 2.5 wt% aligns with the SEM observations (Section 3.2.2), where the same formulation exhibited the highest cell density and smallest cell size. The micro-CT results therefore reinforce the role of BC as an effective heterogeneous nucleating agent, with increased concentration leading to more nucleation sites, more uniformly distributed carbon domains, and a more refined cellular architecture. Together, these 2D and 3D reconstructions confirm the successful incorporation of BC and highlight the structural differences between low and moderate BC loadings.

3.4   Thermal and mechanical performance

The variation of thermal conductivity of PS–BC composite foams with increasing BC loading is presented in Fig. 7. The thermal conductivity decreased from approximately 36 mW m^{-1} K^{-1} for pristine PS to a minimum value of around 32 mW m^{-1} K^{-1} at 2.5 wt% BC, beyond which it gradually increased with further addition of BC. The lowest thermal conductivity observed at 2.5 wt% BC can be directly correlated with the foam's small cell size, narrow cell size distribution, and high cell density, indicating an optimized balance between heterogeneous nucleation and cell growth during sc-CO$_2$ foaming. Enhanced nucleation efficiency at this composition promoted uniform gas bubble formation, which possibly reduced the effective heat transfer pathways within the foam matrix by limiting gas conduction and radiative heat transport.[52] The observed reduction in thermal conductivity at intermediate BC loadings also corresponds to the measured open-cell content values, which decreased remarkably

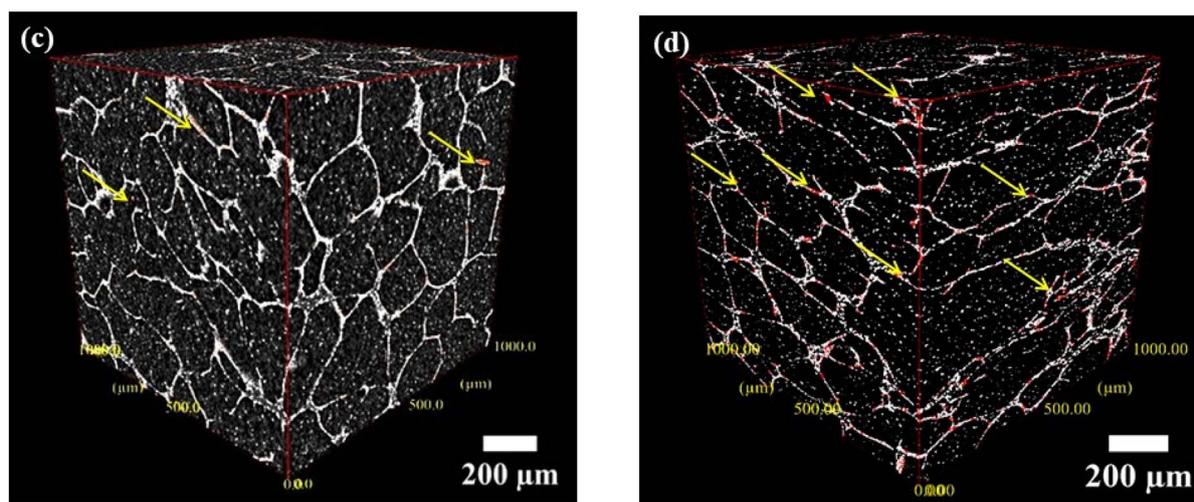## 2D cross-sections
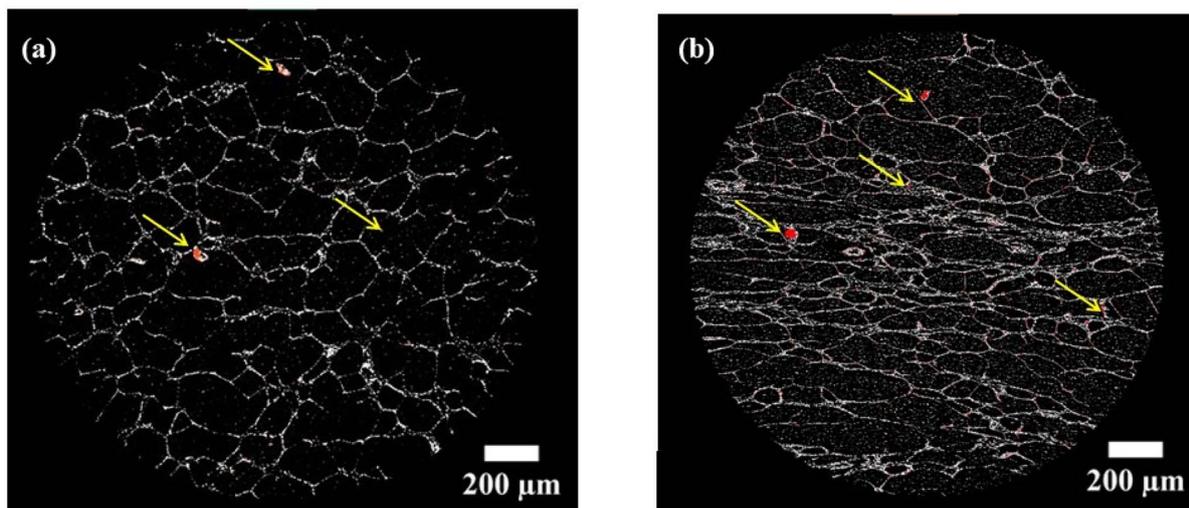
3D volume rendering models

Fig. 6 Reconstructed (a and b) 2D micro-CT cross-sections and (c and d) 3D volume renderings of PS–BC composite foams containing (a and c) 1 wt% BC and (b and d) 2.5 wt% BC (note: yellow arrows indicate high-attenuation regions (red) corresponding to carbon-rich BC particles).

from 45.8% (1 wt%) to 18.8% (2.5 wt%) and remained low at higher BC loadings (13.5–17.6%). The decreased open-cell fraction suggests that the improved nucleation and cell-wall stability at optimized BC loadings effectively could have trapped the CO_2 blowing agent within closed cells. This closed-cell morphology, coupled with the inherently low thermal conductivity of the BC filler itself contributed to the enhanced insulation efficiency of the PS–BC foams. Several previous studies have similarly reported that an increase in the proportion of closed cells is associated with a reduction in the overall thermal conductivity of polymer foams.[48,53]

When compared to the PS-1 GNP/FG (graphene nanoplatelets/flaked graphite) foam reported in our previous work, the PS–BC foam exhibited a similar thermal conductivity, demonstrating that BC incorporation can achieve comparable thermal insulation performance while offering significant

environmental advantages. The use of BC not only displaces fossil-derived carbon fillers but also sequesters biogenic carbon in long-lived polymer products, providing a dual benefit of performance improvement and carbon sequestration. The enhancement in thermal insulation efficiency directly translates to greater energy savings over the lifetime of buildings and contributes to achieving LEED certification and the development of low-carbon, sustainable buildings. Consequently, this work advances the objectives of the United Nations Sustainable Development Goals (SDG 11: Sustainable Cities and Communities; SDG 13: Climate Action) by reducing operational energy demands and associated greenhouse gas emissions through the use of sustainable, carbon-sequestering insulation materials.

The variation of compressive performance of PS–BC composite foams with different BC loadings is presented in Fig. 8. The bar graphs represent the absolute compressive

© 2026 The Author(s). Published by the Royal Society of Chemistry

Table 2 Volume fraction (%) of PS matrix and BC in foamed PS composites from micro-CT analysis

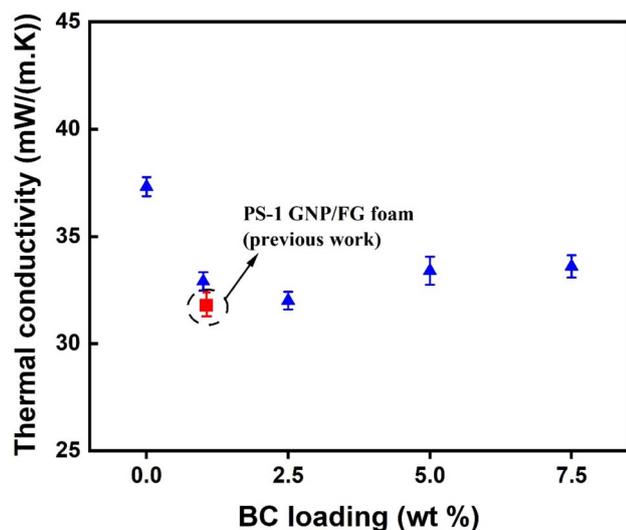| Sample name	Volume fraction of PS matrix (%)	Volume fraction of BC (%)
1 wt% BC	3.0	0.2
2.5 wt% BC	3.9	0.8

Fig. 7 Variation in thermal conductivity of PS composite foams at different BC loadings.

modulus and strength, while the data points correspond to the specific compressive modulus and specific compressive strength, normalized with respect to foam density to better reflect the intrinsic stiffness and load-bearing capability of lightweight foams. A non-monotonic trend was observed in both specific modulus and strength with increasing BC loading.

The highest specific compressive modulus was obtained at 1 wt% BC, which can be correlated with its relatively low foam density (85.6 kg m^{-3}). At this composition, BC particles acted as effective reinforcing fillers and nucleation sites, enhancing stress transfer between the polymer matrix and the dispersed carbon phase. Similarly, the specific compressive strength showed its maximum at 1 wt% (4.1 MPa g^{-1} cm^3) and 2.5 wt% BC (3.9 MPa g^{-1} cm^3), indicating that these loadings provided the most efficient balance between cell morphology and filler dispersion. The enhanced specific compressive strength value for the 2.5 wt% BC foam can be attributed to its small and uniformly distributed cells, as observed in the SEM micrographs. A narrow cell size distribution promotes homogeneous stress distribution under compressive loading, minimizing local stress concentrations and micro-buckling effects in the foam struts.[54] Consequently, this morphology leads to improved specific mechanical performance. At higher loadings ($\geq$5 wt%), both the specific modulus and specific strength decreased, possibly due to BC agglomeration, which disrupted uniform stress transfer and acted as defect sites within the polymer matrix, thereby compromising the foam's mechanical integrity. When compared to the PS-1 GNP/FG foam from our previous work,[55] the PS–2.5 wt% BC composite foam exhibited an even higher specific compressive strength. This result suggests that BC can not only match but exceed the mechanical performance of conventional carbon fillers while offering substantial sustainability advantages.

3.5 Environmental and performance comparison with existing PS foam insulation systems

3.5.1 Performance comparison. Table 3 summarizes mechanical, thermal and environmental performance for PS–BC composite foams with previously reported PS–carbon filler foams and commercial PS insulation products. The PS–2.5 wt% BC foam demonstrates the high specific compressive strength (3.9 MPa g^{-1} cm^3), outperforming some of the conventional
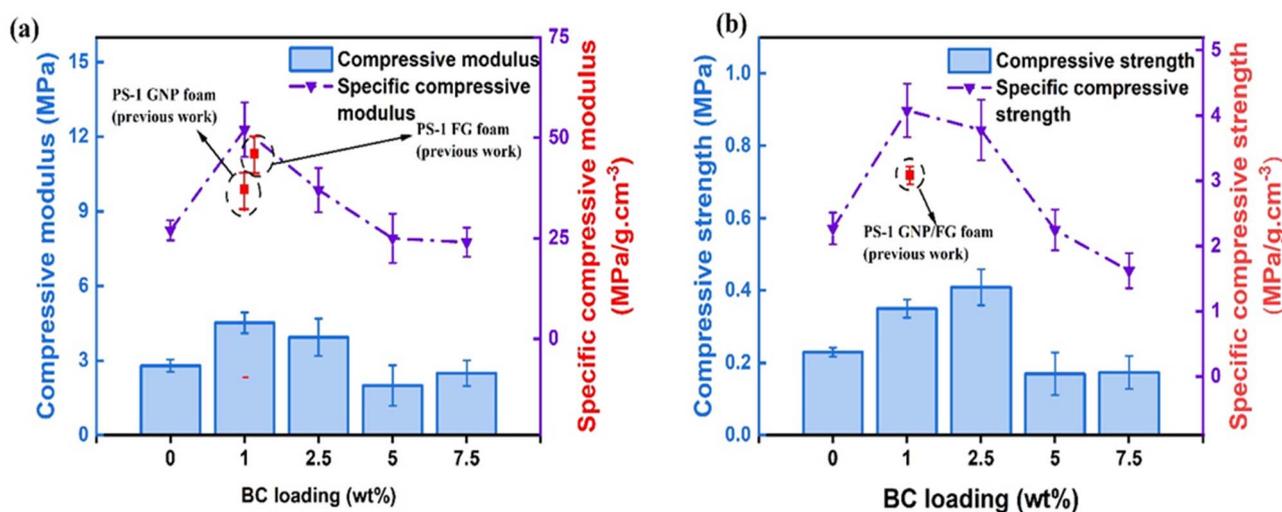

Fig. 8 Compression performance of PS composite foam at varying loadings of BC (a) specific compressive modulus, (b) specific compressive strength.

Table 3 Comparison of mechanical, thermal and environmental performance for PS–BC composite foams with previously reported PS–carbon filler foams and commercial PS insulation products[a]

Product	Specific compressive modulus (MPa g^{-1} cm^3)	Specific compressive strength (MPa g^{-1} cm^3)	Thermal conductivity (mW m^{-1} K^{-1})	R-Value (inch per BTU·in per h ft2 °F)	Total GWP (kg CO$_2$-eq. per kg)	GWP per R-value (kg CO$_2$-eq. per R)
PS-2.5 wt% BC	37	3.9	32.0	4.6	2.7	0.6
PS-1 wt% FG[55]	40	3.8	32.1	4.5	2.9	0.6
PS-1 wt% GNP[55]	33	3.5	32.3	4.4	3.9	0.8
PS-1 wt% coconut shell AC[29]	20.2	—	34.3	4.2	2.8	0.6
PS-1 wt% wood AC[56]	—	10.0	33.9	4.2	2.8	0.6
SOPRA-XPS 30 (ref. 57)	—	6.2	28.8	5.0	2.9	0.6
Greenguard GGS 25-LG[58]	—	5.3	28.8	5.0	4.8	1.0
Islofoam R plus[59]		3.1	31.2	4.6	3.2	0.7
Dupont Styrofoam[60]		5.3	26.5	5.4	10.6	1.9
Durospan GPS[61]		3.5	30.8	4.7	3.1	0.6

[a] AC: activated carbon, FG: flaked graphite, GNP: graphene nanoplatelets, conversions used for calculating R-value are 1 W m^{-1} K^{-1} = 6.94 BTU in per h ft2 °F, GWP values represent cradle-to-gate embodied emissions (kg CO$_2$-eq. per kg) from material production, obtained from reported literature and LCA data).

insulation foam products, which typically exhibit values below 6 MPa g^{-1} cm^3. The specific compression modulus of PS–BC composite foam produced in this work exceeded PS-FG and GNP foam from our previous work while achieving a similar thermal conductivity. A further reduction in foam density, without compromising cell integrity, would likely enhance the specific compressive strength and modulus values, advancing these materials toward the performance range of lightweight commercial PS foam products. The measured thermal conductivity of (32 mW m^{-1} K^{-1}) and corresponding R-value (4.6) are comparable to those of leading extruded polystyrene (XPS) products ($R \approx 5.0$), indicating that the BC-filled foams achieve similar insulation efficiency while offering improved stiffness-to-weight performance. These findings highlight the potential of renewable BC as a partial replacement for synthetic fillers in PS insulation foams without compromising thermal insulation capability.

3.5.2 Environmental and sustainability impact

3.5.2.3 Global warming potential (GWP) estimation approach. In this study, the Global Warming Potential (GWP) values reported for materials such as PS, fillers (BC, graphite), and flame retardants refer to their cradle-to-gate-embodied greenhouse gas emissions. These values quantify the total CO$_2$-equivalent emissions (kg CO$_2$-eq. per kg material) associated with raw material extraction, processing, and manufacturing, as reported in literature and LCA databases. The total material-related GWP of each foam formulation was estimated using a component-wise summation approach, considering the contribution of each raw material to the total foam composition. GWP values (kg CO$_2$-eq. per kg) for individual components, including virgin PS, blowing agents (CO$_2$, HFOs, HFCs), flame retardants, fillers (BC, graphite, talc), and additives were obtained from published LCA databases and literature sources (see SI, Table S2). The approximate composition of commercial XPS products (*e.g.*, SOPRA-XPS, STYROFOAM, Greenguard GGS 25-LG, Durospan

GPS) was derived from technical data sheets (TDS) and patent disclosures (Table S3). The total material GWP for each foam was then calculated as:

$$\text{GWP}_{\text{total}} = \sum_i (w_i \times \text{GWP}_i)$$

where w_i is the mass fraction of component i in the foam formulation and GWP$_i$ is its respective cradle-to-gate global warming potential. The GWP was further normalized by the foam's thermal resistance (R-value) to enable direct comparison of environmental efficiency among materials. Detailed calculations, assumptions, and individual GWP sources are provided in the SI.

A comparative analysis of the material GWP and corresponding GWP per thermal resistance unit (R-value) highlighted the environmental advantages of the PS-2.5 wt% BC composite foam relative to both commercial and previously reported PS foam insulation materials (Table 3). The PS-2.5 wt% BC foam exhibits one of the lowest total embodied carbon values (2.8 kg CO$_2$ eq. per kg) and the lowest GWP normalized by R-value (0.6 kg CO$_2$ eq. per R) among all compared foams. These values are significantly lower than those of representative commercial XPS boards such as Styrofoam XPS (1.9 kg CO$_2$ eq. per R) and Greenguard GGS 25-LG (1 kg CO$_2$ eq. per R). Although the BC loading is modest, the partial substitution of virgin PS with low-GWP, biogenic BC effectively reduced the material carbon footprint while maintaining comparable thermal insulation and mechanical performance. Moreover, BC contributes to carbon sequestration, as its fixed carbon originates from atmospheric CO$_2$ captured by biomass. When retained within the foam matrix, this biogenic carbon remains locked over the product lifetime and could generate additional carbon-credit value for foam manufacturers. Consequently, even without a full LCA, the side-by-side GWP–R-value comparison provided quantitative evidence that the incorporation of BC enhances

© 2026 The Author(s). Published by the Royal Society of Chemistry

both the environmental sustainability and potential economic viability of PS–BC composite insulation foams.

4 Conclusions

The incorporation of wood-derived biochar (BC) into PS foams *via* sc-CO$_2$ extrusion successfully produced lightweight, mechanically robust, and thermally efficient composite insulation materials. BC acted as an effective heterogeneous nucleating agent, as evidenced by uniform dispersion and preferential localization along the polymer cell walls observed in TEM images. Micro-CT reconstructions further verified greater BC incorporation and structural uniformity at 2.5 wt%, consistent with its superior cellular morphology. Among all formulations, the foam containing 2.5 wt% BC exhibited the most refined and homogeneous cellular structure, with an average cell size of ∼86 μm, a high cell density of ∼3.3 × 10^8 cells per cm^3, and a narrow size distribution. These optimized microstructural features translated into enhanced macroscopic properties, reducing thermal conductivity from ∼36 to ∼32 mW m^{-1} K^{-1} (≈11% reduction) and doubling the specific compressive strength to 3.9 MPa g^{-1} cm^3 compared to pristine PS foam. This demonstrates that a modest BC loading of 2.5 wt% can effectively improve foam nucleation, structural integrity, and overall thermal–mechanical performance without compromising processability.

Beyond property enhancement, BC incorporation substantially improved the environmental profile of the composite foams. Comparative embodied carbon and thermal resistance analyses revealed lower total GHG emissions and reduced GWP per unit insulation performance, confirming the role of BC in displacing fossil carbon with renewable, biogenic carbon. The fixed carbon content of BC contributes to long-term carbon sequestration within the foam matrix, offering potential for additional climate benefits over the product lifetime. By integrating a renewable, carbon-rich additive with a clean, solvent-free sc-CO$_2$ foaming process, this work advances a scalable approach toward circular material use in polymer foams. The resulting PS–BC composites align strongly with the United Nations Sustainable Development Goals (SDG 11: Sustainable Cities and Communities, and SDG 13: Climate Action), representing a practical and sustainable pathway for developing next-generation low-carbon insulation materials.

Author contributions

Apurv Gaidhani: conceptualization, methodology, investigation, visualization, data curation, writing – original draft; Guoshan Min: data curation, writing – review & editing; Lauren Tribe: writing – review & editing, supervision, methodology, validation, funding acquisition, writing – review & editing; Paul Charpentier: writing – review & editing supervision, methodology, validation, funding acquisition.

Conflicts of interest

There are no conflicts to declare.

Data availability

The data supporting the findings of this study are included within the manuscript and the supporting information (SI). Supplementary information is available. See DOI: https://doi.org/10.1039/d5su00884k.

References

1 M. Aksit, C. Zhao, B. Klose, K. Kreger, H. W. Schmidt and V. Altstädt, *Polymers*, 2019, **11**, 268.
2 P. Li, H. Zhang and L. Chen, *Polymers*, 2025, **17**, 1606.
3 K. Voith, B. Spisák, M. Petrik, Z. Szamosi and G. L. Szepesi, *Processes*, 2023, **11**, 12.
4 H. Yoshihara and M. Maruta, *Polymers*, 2020, **12**, 47.
5 C. V. Vo and A. N. Paquet, *J. Cell. Plast.*, 2004, **40**, 205–228.
6 A. M. Borrero-López, V. Nicolas, Z. Marie, A. Celzard and V. Fierro, *Polymers*, 2022, **19**, 3974.
7 L. Doyle, I. Weidlich and E. Di Maio, *Materials*, 2022, **15**, 6212.
8 Resources Canada N, *Keeping the Heat In*, 2025, https://natural-resources.canada.ca/energy-efficiency/home-energy-efficiency/keeping-heat, accessed on 30th December 2025.
9 S. Danov, J. Carbonell, J. Cipriano and J. Martí-Herrero, *Energy Build*, 2013, **57**, 110–118.
10 H. X. Zhao and F. Magoulès, *Renewable Sustainable Energy Rev.*, 2012, 3586–3592, DOI: 10.1016/j.rser.2012.02.049.
11 J. R. Zhao, R. Zheng, J. Tang, H. J. Sun and J. Wang, *J. Hazard. Mater.*, 2022, 129449, DOI: 10.1016/j.jhazmat.2022.129449.
12 Tracking buildings, https://www.iea.org/energy-system/buildings, accessed 7 August 2025.
13 L. Pérez-Lombard, J. Ortiz and C. Pout, *Energy Build*, 2008, **40**, 394–398.
14 S. B. Sadineni, S. Madala and R. F. Boehm, *Renewable Sustainable Energy Rev.*, 2011, **15**, 3617–3631.
15 J.-F. Côté, *Environmental Impact of Extruded Polystyrene and Other Insulation Used in Buildings*.
16 Green Theory, *Expanded Polystyrene and Styrofoam – Environmental Impact and Solutions*.
17 K. H. H. Aziz, Biochar, hydrochar, and their derivative composites for heavy metal adsorption, *Composites and Biocomposites for Heavy Metal Adsorption*, Woodhead Publsihing, 2026, pp. 53–72.
18 K. H. H. Aziz, *Desalin. Water Treat.*, 2024, **320**, 100757.
19 R. Kareem, A. Afkhami and K. H. H. Aziz, *RSC Adv.*, 2025, **15**, 20309–20320.
20 R. N. Noori, D. F. Hamamin and K. H. H. Aziz, *J. Dispersion Sci. Technol.*, 2025, 1–13.

21 O. Das, A. K. Sarmah and D. Bhattacharyya, *Waste Manage.*, 2016, **49**, 560–570.

22 S. Gupta and H. W. Kua, *J. Mater. Civ. Eng.*, 2017, **29**, DOI: 10.1061/(asce)mt.1943-5533.0001924.

23 A. Ulusal, E. Apaydın Varol, V. J. Bruckman and B. B. Uzun, *Biomass Convers. Biorefin.*, 1041–1051, DOI: 10.1007/s13399-020-00923-7.

24 A. Gaidhani, L. Tribe and P. Charpentier, *J. Cell. Plast.*, 2023, **59**, 419–453.

25 L. Yee Foong Ng, H. Ariffin, T. A. Tengku Yasim-Anuar, M. Sakata, T. Kawarada, O. Yoshimura, T. Tsukegi, N. M. Afizan Nik Abd Rahman and M. A. Hassan, *RSC Adv.*, 2024, **14**, 21971–21981.

26 D. Cuthbertson, U. Berardi, C. Briens and F. Berruti, *Biomass Bioenergy*, 2019, **120**, 77–83.

27 Q. Zhang, H. Cai, X. Ren, L. Kong, J. Liu and X. Jiang, *Polymers*, 2017, **9**, 628.

28 J. George, S. Gaidukovs and D. Bhattacharyya, *Int. J. Smart Nano Mater.*, 2024, **15**, 767–785.

29 L. Jian, T. Fan, M. Weng, W. Yu, W. Chen, J. Luo, J. Liang, Y. Min and R. Wang, *Diam. Relat. Mater.*, 2022, **130**, 109495.

30 S. M. Desjardins, M. T. Ter-Mikaelian and J. Chen, *BioChar*, 2024, **6**, 58.

31 J. Carvalho, L. Nascimento, M. Soares, N. Valério, A. Ribeiro, L. Faria, A. Silva, N. Pacheco, J. Araújo and C. Vilarinho, *Processes*, 2022, **10**, 2684.

32 H. Haham, A. Riscoe, C. W. Frank and S. L. Billington, *Appl. Surf. Sci. Adv.*, 2021, **3**, 100059.

33 C. Botta, C. M. Grottola, D. Amato and M. R. Acocella, *Polymers*, 2024, **16**, 3347.

34 K. Uram, M. Kurańska, J. Andrzejewski and A. Prociak, *Materials*, 2021, **14**, 5616.

35 R. Banerjee and S. S. Ray, *Macromol. Mater. Eng.*, 2020, 2000366, DOI: 10.1002/mame.202000366.

36 H. Y. Mi, X. Jing and L. S. Turng, *J. Cell. Plast.*, 2014, **51**, 165–196.

37 M. Dong, G. Wang, X. Zhang, D. Tan, D. Jaya Prasanna Kumar, J. Ren, H. Colorado, H. Hou, Z. Toktarbay and Z. Guo, *Adv. Compos. Hybrid Mater.*, 2023, 207, DOI: 10.1007/s42114-023-00790-6.

38 A. Gaidhani, G. Min, W. Z. Xu, L. Tribe and P. Charpentier, *Polym. Eng. Sci.*, 2025, **65**, 4170–4185.

39 D. Matykiewicz, *Processes*, 2020, **8**, 1–13.

40 R. R. Domingues, P. F. Trugilho, C. A. Silva, I. C. N. A. De Melo, L. C. A. Melo, Z. M. Magriotis and M. A. Sánchez-Monedero, *PLoS One*, 2017, e0176884.

41 S. Gezahegn, M. Sain and S. C. Thomas, *Soil Syst.*, 2019, **3**, 1–16.

42 W. Barszcz, M. Łożyńska and J. Molenda, *Sci. Rep.*, 2024, **14**, 10501.

43 J. Bedia, M. Peñas-Garzón, A. Gómez-Avilés, J. J. Rodriguez and C. Belver, *C*, 2018, **4**, 63.

44 M. Keiluweit, P. S. Nico, M. Johnson and M. Kleber, *Environ. Sci. Technol.*, 2010, **44**, 1247–1253.

45 S. Jurczyk, J. Andrzejewski, A. Piasecki, M. Musioł, J. Rydz and M. Kowalczuk, *Polymers*, 2024, **16**, 1231.

46 Z. Chen, X. Yin, H. Chen, X. Fu, Y. Sun, Q. Chen, W. Liu and X. Shen, *Polymers*, 2024, **16**, 28.

47 L. D. Hung Anh and Z. Pásztory, *J. Build. Eng.*, 2021, 102604, DOI: 10.1016/j.jobe.2021.102604.

48 O. V. Soloveva, S. A. Solovev, Y. V. Vankov and R. Z. Shakurova, *Processes*, 2022, **10**, 2257.

49 J. S. Colton and N. P. Suh, *Polym. Eng. Sci.*, 1987, **27**, 493–499.

50 J. Colton and N. Suh, *Polym. Eng. Sci.*, 1987, **27**, 482–492.

51 L. Yee Foong Ng, H. Ariffin, T. A. Tengku Yasim-Anuar, M. Sakata, T. Kawarada, O. Yoshimura, T. Tsukegi, N. M. Afizan Nik Abd Rahman and M. A. Hassan, *RSC Adv.*, 2024, **14**, 21971–21981.

52 P. Gong, P. Buahom, M. P. Tran, M. Saniei, C. B. Park and P. Pötschke, *Carbon*, 2015, **93**, 819–829.

53 S. R. Shin and D. S. Lee, *Nanomaterials*, 2022, **12**, 685.

54 J. Chen, L. Yang, D. Chen, Q. Mai, M. Wang, L. Wu and P. Kong, *Cell. Polym.*, 2021, **40**, 101–118.

55 A. Gaidhani, S. Edwards, L. Tribe and P. Charpentier, *J. Thermoplast. Compos. Mater.*, 2025, DOI: 10.1177/08927057251401189.

56 C. Zhang, B. Zhu and L. J. Lee, *Polymer*, 2011, **52**, 1847–1855.

57 SOPREMA, *SOPRA-XPS 30 Technical Data Sheet*, SOPREMA Inc., available at https://www.soprema.ca/en/products-systems/sopra-xps-30, accessed 10th December 2025.

58 K. Insulation, *LS-XPS-Insulation Board Line Sheet*, K. Insulation (General Insulation), available at https://www.generalinsulation.com/wp-content/uploads/2019/06/GreenGuard-XPS-Insulation-Board-Line-Sheet.pdf, accessed 8th December 2025.

59 Isolofoam Group, *ISO R Plus premium Technical Data Sheet*, Isolofoam Group, available at https://isolofoam.com/wp-content/uploads/2019/10/Isolofoam_ISO-R-PLUS-premium_TDS_EN_2016-12_2.3.pdf, accessed 10th December 2025.

60 DuPont, *DuPont™ Styrofoam™ Brand Ultra SL XPS Insulation Product Information Sheet*, DuPont, available at https://www.dupont.com/content/dam/dupont/amer/us/en/performance-building-solutions/public/documents/en/styrofoam-brand-ultra-sl-xps.pdf, accessed 12th December 2025.

61 Plastifab, *DuroSpan® GPS R5 Insulation*, Plastifab Inc., available at https://www.plastifab.com/products/durospan-gps-insulation/durospan-gps-r5.html, accessed 11th December 2025.